Sensitivity of Rotor Blade Vibration Characteristics to Torsional Oscillations

Theodore Bratanow* and Akin Ecer†
University of Wisconsin-Milwaukee, Milwaukee, Wis.

A theoretical investigation of dynamic response characteristics of helicopter rotor blades in forward flight was carried out with special emphasis on the torsional degrees-of-freedom. The finite element method was applied in the formulation of the coupled equations of motion for flapwise bending and torsion for blades with noncolinear elastic, mass, and aerodynamic axes. The sensitivity of blade vibration characteristics with respect to several basic structural, geometric, and aerodynamic properties as well as flight conditions was evaluated. Numerical results for sample blades were plotted to show the variation of the coupling between bending and torisonal components of the response.

Nomenclature

a = lift curve slope for normal flow
B_1, B_2 = arbitrary scalars
$C_{\theta i}$ = generalized control element stiffness in torsion
$\mathbf{D}_s$ = structural damping matrix
$\mathbf{D}_a(\Psi)$ = aerodynamic damping matrix
EI = bending stiffness of a blade, lbf-in.^{2} (N-m^2)
$F_i(\Psi)$ = generalized force in bending, lbf (N)
$\mathbf{F}(t)$ = external load vector, lbf (N)
$G(\Psi)$ = control moment in torsion, lbf-in. (N-m)
$\mathbf{G}(t)$ = external load vector, lbf (N)
h = vertical displacement of a blade at the elastic center, in. (m)
H_i = aerodynamic loading in bending
I_θ = torsional inertia of the rotor blade, lbf-sec^2 (N-sec^2)
JG = torsional stiffness of a blade, lbf-in.^{2} (N-sec^2)
$\mathbf{K}_s$ = structural stiffness matrix
$\mathbf{K}_a(\Psi)$ = aerodynamic stiffness matrix
m = mass of the blade per unit length, lbf-sec^2/in.^{2} (N-sec^2/m^2)
$m_{ij}(\Psi)$ = generalized coupled torsional stiffness in bending, lbf-in.^{2} (N-m)
$\mathbf{M}_a(\Psi)$ = aerodynamic mass matrix
$\mathbf{M}_s$ = structural mass matrix
p = a scalar [see Eq. (9)]
$p_{ij}(\Psi)$ = generalized torsional damping in torsion, lbf-sec/rad (N-sec/rad)
$P_{ij}(\Psi)$ = generalized bending damping in bending, lbf-sec/in. (N-sec/m)
q = frequency ratio [see Eq. (9)]
$q_{ij}(\Psi)$ = generalized torsional stiffness in torsion, lbf/rad (N/rad)
$Q_{ij}(\Psi)$ = generalized bending stiffness in bending, lbf/in. (N/m)
r = distance of rotor blade element from center of rotation, in. (m)
$\mathbf{r}$ = coupled displacement vector, in. (m)
R = rotor radius, in. (m)
R_{ij} = generalized coupled bending stiffness in torsion, lbf/in. (N/m)
S = nondimensionalized eccentricity, [see Eq. (9)]
S_{ij} = generalized coupled bending damping in torsion, lbf-sec/rad (N-sec/rad)
T = centrifugal force along the longitudinal axis of rotating blade, lbf (N)
T_i = aerodynamic loading in torsion
U = total energy, lbf-in. (N-m)
x_θ = eccentricity between the elastic and mass center, in. (m)
X_i = generalized bending deflection at blade tip, in. (m)
Y_i = generalized torsional rotation at blade tip, in. (m)
α_i = structural mass coefficient
β_i = structural damping coefficient
γ_i = structural stiffness coefficient
η = ratio of torsional rotations to bending displacement in the vibration mode corresponding to the lowest frequency, rad/in. (rad/m)
θ = pitch due to blade torsion, rad
κc = distance between elastic axis and center of pressure in reversed flow region, in. (m)
λ = square of the ratio of lowest torsional frequency to the lowest bending frequency
μ = tip-speed ratio
Ψ = azimuth angle, rad
ω_i = natural frequency of a blade, rad/sec
Ω = angular velocity of a rotating blade, rad/sec

Subscripts

B = bending
G = at the center of gravity
T = torsion

Introduction

TORSIONAL oscillations become an important consideration in determining the dynamic response characteristics of rotor blades at high forward speeds. In general, the analysis of the response under actual flight conditions represents a complicated problem because of the three-dimensional nature of the blade deformations and the unsteady flow conditions around rotating blades. Increased forward speed and higher maneuverability requirements further increase the complexity of the problem.

The objectives of the conducted research were to evaluate the sensitivity of dynamic response characteristics of rotor blades to torsional oscillations, and to determine means of controlling these torsional oscillations by changing structural, geometric, and aerodynamic properties of rotor blades. The analysis is presented in two parts: evaluation of the importance of torsional oscillations for different conditions and variation of blade parameters to improve blade response and stability in coupled bending and torsion.

Method of Analysis

The equations of motion of a rotor blade in forward flight were formulated from a discrete mass-stiffness representation of the blade and the airloads using the finite element method. Considering the aerodynamic loading as

Presented as Paper 73-404 at the AIAA/ASME/SAE 14th Structures, Structural Dynamics, and Materials Conference, Williamsburg, Va., March 20–22, 1973; submitted April 2, 1973; revision received April 16, 1974. This research was supported by NASA under Grant NGR-50-007-001.

Index categories: Rotary Wing Aerodynamics; VTOL Vibration.

*Professor of Engineering Mechanics. Member AIAA.

†Assistant Professor of Engineering Mechanics. Member AIAA.

a forcing function, the equations of motion were first written as

$$M_s\ddot{r} + D_s\dot{r} + K_s r = F(t) \tag{1}$$

This system was then expanded by including the aerodynamic mass, damping, and stiffness properties as functions of blade azimuth positions

$$[M_s + M_a(\Psi)]\ddot{r} + [D_s + D_a(\Psi)]\dot{r} + [K_s + K_a(\Psi)]r = G(t) \tag{2}$$

The sensitivity analysis was then performed on both systems, Eqs. (1) and (2). The variations of frequencies and coupling between the bending and torsional components of the dynamic response were determined as functions of structural and aerodynamic parameters.

Sensitivity of Structural Vibration Characteristics of Rotor Blades

An energy formulation was applied to determine the importance of the coupling between structural mass and stiffness parameters in terms of the eccentricity between elastic and mass axes. The total energy of the blade motion for the uncoupled case consists of

$$U_B = \frac{1}{2}\int_0^R (EIh''^2 - \omega_B{}^2 mh'^2 + Th'^2)dr \tag{3}$$

in bending and

$$U_T = \frac{1}{2}\int_0^R (JG\theta'^2 - \omega_T{}^2 I_\theta\theta^2 + \Omega^2 I_\theta\theta^2)dr \tag{4}$$

in torsion. For the coupled motion of the blade, and for small values of θ, the displacements at the center of mass of the blade can be defined as

$$h_G = h + x_\theta\theta \tag{5}$$

Substituting Eq. (5) into Eqs. (3) and (4), the total energy for the coupled motion of the rotor blade in bending and torsion can be written as

$$U = \frac{1}{2}\int_0^R (EIh''^2 - \omega^2 m(h + x_\theta\theta)^2 + T(h + x_\theta\theta)'^2 + JG\theta'^2 - \omega^2 I_\theta\theta^2 + \Omega^2 I_\theta\theta^2)dr \tag{6}$$

The finite element method was employed to determine the mass and stiffness matrices of the rotor blade from Eq (6).[1] From the finite element formulation one can easily determine the importance of different distributions of eccentricity along the blade axis on the coupled frequencies and the torsional oscillations at lower frequencies.

An approximate analysis of the coupled behavior can be accomplished by substituting Eqs. (3) and (4) into Eq. (6) and obtaining

$$U = \frac{1}{2}\int_0^R [(\omega_B{}^2 - \omega^2)mh^2 + (\omega_T{}^2 - \omega^2)I_\theta\theta^2 - \omega^2 m\theta^2 x_\theta{}^2 - \omega^2 m\theta x_\theta h + Tx_\theta{}^2\theta'^2 + 2Tx_\theta\theta'h']dr + U_B + U_T \tag{7}$$

By assuming a two-degree-of-freedom system, where the bending and torsional modes are

$$h = B_1 x \quad \text{and} \quad \theta = B_2 x = \eta B_1 x \tag{8}$$

one can obtain

$$S_1 = \frac{x_\theta{}^2 m}{I_\theta} = \frac{\left(\frac{\omega^2}{\omega_{B1}{}^2} - 1\right)\left(\frac{\omega^2}{\omega_{B1}{}^2} - \frac{\omega_{T1}{}^2}{\omega_{B1}{}^2}\right)}{\left(\frac{\Omega^2}{\omega_{B1}{}^2} - \frac{\omega^2}{\omega_{B1}{}^2}\right)\left(\frac{\Omega^2}{\omega_{B1}{}^2} - 1\right)} = \frac{(q-1)(q-\lambda)}{(p-q)(p-1)} \tag{9}$$

As the nondimensional eccentricity between mass and elastic axes increases, the lower of the two frequencies, which corresponds to a predominantly bending mode, decreases slightly, while the torsional frequency increases. For zero eccentricity ($S = 0$), two uncoupled frequencies correspond to $q = 1$ and $q = \lambda$. As the coupling increases the coupled bending frequencies are bound between

$$\omega_{B1}{}^2 < \omega^2 < \Omega^2 \tag{10}$$

By approximating the variation of frequencies in this region by a linear curve and assuming that

$$\omega_{T1}{}^2 >> \omega^2 \tag{11}$$

the following relationship can be derived from Eq. (9)

$$\eta\alpha\frac{m}{I_\theta}\frac{\omega_{B1}}{\omega_{T1}}x_\theta \tag{12}$$

Another consideration is the importance of the second-order terms in x_θ in Eq. (6). These terms represent the change in the moment of inertia of the blade due to an eccentricity between elastic and mass axes. Neglecting the second-order terms, Eq. (9) becomes

$$S_2 = \frac{(q-1)(q-\lambda)}{(p-q)(p-q)} \tag{13}$$

Equations (9) and (13) are plotted in Fig. 1. In this case the coupled mass matrix becomes singular at

$$\frac{x_\theta{}^2 m}{I_\theta} = 1 \tag{14}$$

and the system is unstable for values of $S > 1$. It is important to consider this singularity when using the equations of motion of rotor blades[2] as a basis of dynamic response and stability analysis.

A sample blade (CH-34) was chosen to illustrate the coupled behavior of a rotor blade considering only structural properties. From the multi-degree-of-freedom finite element model the frequencies and coupling between bending and torsional displacements were calculated for different eccentricities in the blade. Obtained results[1] agreed with the behavior predicted in Fig. 1. The sample blade was analyzed for both hinged and fixed-end support conditions. The results are plotted in Figs. 2a–2c and can be interpreted using Eq. (12). The variation of coupled and uncoupled frequencies with increasing rotational speeds is shown in these figures. From these curves one can also observe that the torisonal component of the coupled motion increases linearly with the eccentricity and is proportional to the square of blade rotational speed.

The effects of blade structural properties on coupled response were also investigated. When the weight distribution of the blade was increased by 30%, the bending and torsional frequencies decreased—the first bending frequency by 1.5% and the first torsional frequency by 2.3%. However, in accordance with Eq. (12) the coupling ratio for the lowest frequency increased 30%. Increasing the torsional inertia by 30% resulted in no change in the lowest bending frequency; however, torsional frequencies were decreased as shown in Fig. 3. There was an increase in torsional coupled rotation in the second mode; however, there was no effect on the first mode.[1] These results can also be explained from Eq. (12). The increase in torsional inertia and the resulting decrease in torsional frequency has a balancing effect, producing no increase in coupling. The effect of decreasing torsional frequency however, causes a net increase in coupling for the modes above the first bending mode. The effect of an increase in the torsional rigidity on the frequency is presented in Fig. 3. A 25% reduction of the maximum torsional rotations was obtained in the first coupled mode by increasing the torsional rigidity by 30%. The lower frequencies were not affected, although the predominantly torsional frequencies were increased. Analysis of a one-degree-of-freedom sys-

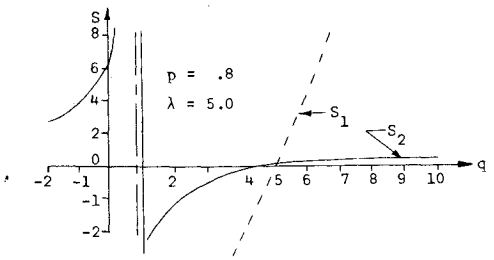

Fig. 1 Variation of coupled frequencies of rotating blades with eccentricities.

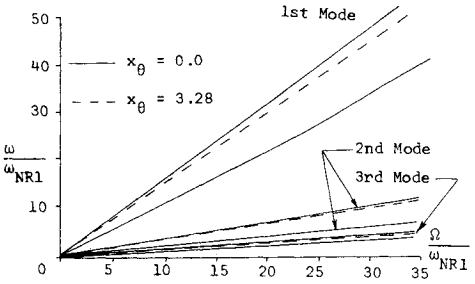

Fig. 2a Variation of lowest bending frequencies for a hinged and a cantilever blade (CH-34) with blade rotational velocity.

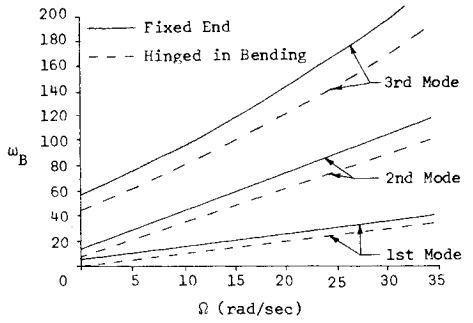

Fig. 2b Variation of lowest bending frequencies for a cantilever and hinged blade (CH-34) with blade rotational velocity.

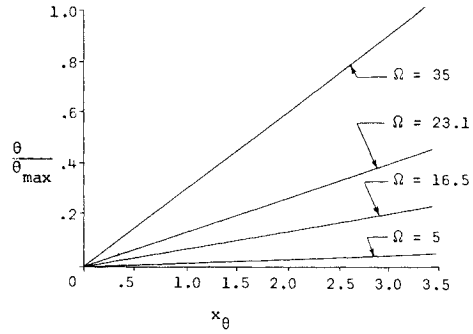

Fig. 2c Variation of the torsional rotations at the blade tip with eccentricity.

tem according to Eq (12) agrees with the plotted results from the finite element model, showing an increase in torsional frequency and a decrease in the torsional component of the lowest bending mode. Increasing the bending moment of inertia by 30% resulted in no change in the bending or torsional frequencies and no variation in the mode shapes. This result confirms the validity of Eq. (12) since coupling is unaffected by a variation of the bending moment of inertia. The above analysis can be performed for any other structural properties of the rotor blade.

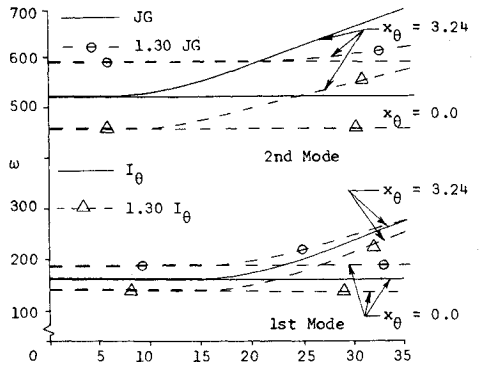

Fig. 3 Variation of torsional frequencies with increasing torsional rigidity and torsional inertia (CH-34).

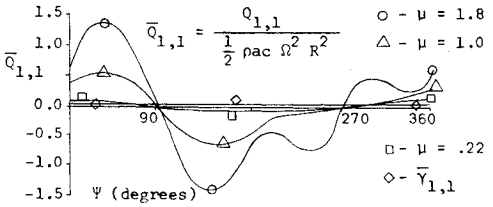

Fig. 4 Aerodynamic stiffness in first bending mode at various advance ratios (μ), (CH-34), ($\kappa = 0.5, x_\theta = 0.0$).

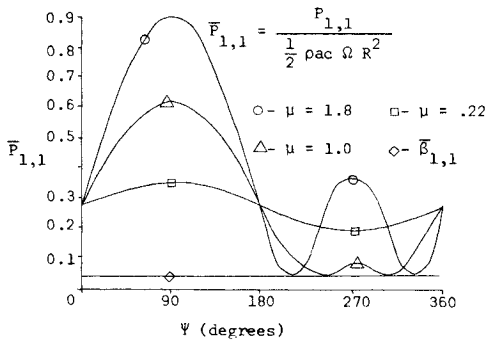

Fig. 5 Aerodynamic damping in first bending mode at various advance ratios (μ), (CH-34 blade), ($\kappa = 0.5, x_\theta = 0.0$).

Aerodynamics of Rotor Blades in Forward Flight

The aerodynamic loading was determined for a particular forward flight condition in terms of blade flapping and torsional motion. The load distribution along the blade was determined for each of the vibration modes calculated from the structural analysis. The resulting aerodynamic loads can be written as

$$H_i = F_i(\Psi) + Y_k m_{ik}(\Psi) + X_j Q_{ij}(\Psi) + \dot{X}_j P_{ij}(\Psi) \quad (15)$$

for flapping and

$$T_i = \dot{Y}_j p_{ij}(\Psi) + C_{\theta i}(\Psi)\dot{\theta}_p + G_i(\Psi) + X_h R_{hi}(\Psi) + \dot{X}_{ki} S_{ki}(\Psi) + Y_j q_{ij}(\Psi) \quad (16)$$

for torsional motion. The variation of the aerodynamic coefficients with blade azimuth position was analyzed in each mode for the sample blade.[1] Each of the terms defined in Eqs. (15) and (16) was plotted for various tip-speed ratios for the mode corresponding to the lowest bending frequency. The aerodynamic bending stiffness, Q_{11}, represents the resultant force in the first coupled structural mode as a result of unit displacement in the same mode and is plotted in Fig. 4. For a tip-speed ratio corresponding to the operating speed of the CH-34 blade ($\mu = 0.22$), the aerodynamic bending stiffness is in the

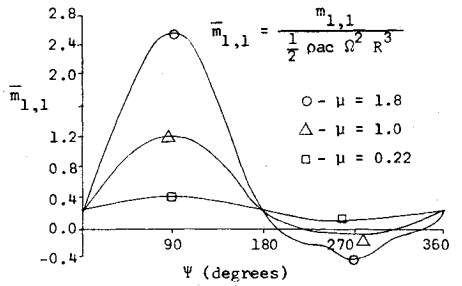

Fig. 6 Aerodynamic stiffness coupling of first torsional and first bending modes at various advance ratios (μ), (CH-34 blade), ($\kappa = 0.5$, $x_\theta = 0.0$).

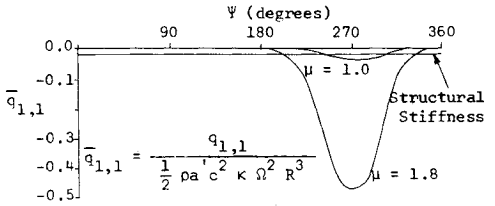

Fig. 7 Aerodynamic stiffness for first torsional mode with various advance ratios (μ), (CH-34 blade), ($\kappa = 0.5$, $x_\theta = 0.0$).

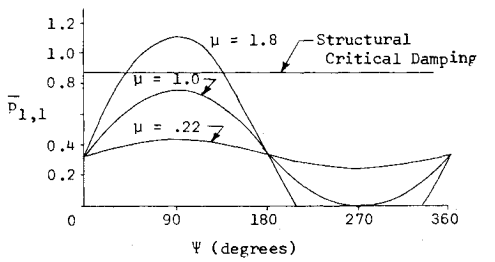

Fig. 8 Aerodynamic damping for first torsional mode with various advance ratios (μ), (CH-34 blade), ($\kappa = 0.5$, $x_\theta = 0.0$).

range of the structural stiffness. For this case the effect of reverse flow is negligible. In general, as the tip-speed increases, the stiffness values show a greater variation with changes in azimuth positions. This variation is greater in the forward flow region and smaller in the reverse flow region. Therefore, for high tip-speed ratios, stability problems may arise in the flapping mode due to the resulting negative bending stiffness.

As shown in Fig. 5, the generalized aerodynamic damping in the first mode, P_{11}, also depends on the tip-speed ratio. For the operating speeds of the CH-34 blade, the aerodynamic damping coefficient is found to have nearly a constant value; however, it varies considerably when the tip-speed ratios are further increased. The damping increases in the forward flow region but nearly vanishes for the reverse flow region. This may be one of the reasons for the existence of increased bending vibrations in the reverse flow region. It should be noted also that the calculated values of aerodynamic damping with respect to the critical structural damping are found to be quite high for rotor blades at high forward speeds. Finally, the aerodynamic stiffness coupling term for the first bending and torsional modes is also dependent on tip-speed ratios. It can be observed from Fig. 6 that the coupling term has a different sign for different flow regions for high tip-speed ratios, but is almost constant for low tip-speed ratios.

The variation of torsional parameters with azimuth angles and tip-speed ratios is shown in Figs. 7–10. Aerodynamic torsional stiffness exists in the reverse flow region. As can be seen from Fig. 7, it acts as a negative feathering spring for this region and increases with increasing tip-

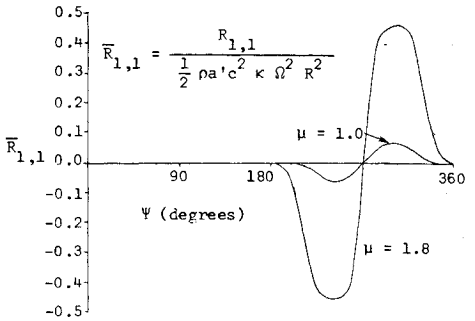

Fig. 9 Aerodynamic stiffness coupling of first bending and first torsional modes at various advance ratios (μ), (CH-34 blade), ($\kappa = 0.5$, $x_\theta = 0.0$).

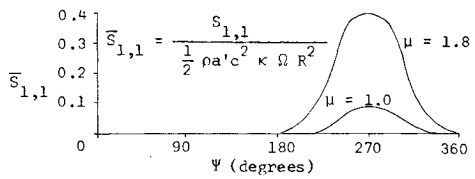

Fig. 10 Aerodynamic damping coupling of first bending and first torsional modes at various advance ratios (μ), (CH-34 blade), ($\kappa = 0.5$, $x_\theta = 0.0$).

speed ratios. Accordingly, the total torsional stiffness of the blade is lower in the reverse flow region. This can be controlled by adjusting the structural torsional stiffness of the blade. The variation of the torsional damping for various tip-speed ratios is shown in Fig. 8. For high tip-speed ratios, considerable torsional damping is obtained for forward flow, while for the reverse flow the aerodynamic damping vanishes. The variations of the coupled aerodynamic stiffness and damping terms are shown in Figs. 9 and 10. These terms exist for the reverse flow and increase with the tip-speed ratios.

Sensitivity of Dynamic Response Characteristics in Forward Flight

The equations of motion of rotor blades in forward flight can be expressed in terms of the generalized aerodynamic and structural mass, damping and stiffness coefficients in bending and torsion as follows:

$$\alpha_{Bi}\ddot{X}_i + (\beta_{Bi} + P_{ij}(\Psi))X_{i,j} + (\gamma_{Bi} + Q_{ij}(\Psi))X_{i,j} + Y_h m_{ih}(\Psi) = L_{ei}(\Psi) \quad (17)$$

$$\alpha_{Ti}\ddot{Y}_i + (\beta_{Ti} + p_{ij}(\Psi))\dot{Y}_{i,j} + (\gamma_{Ti} + q_{ij}(\Psi))Y_{i,j} + R_{ih}(\Psi)X_h + S_{ih}(\Psi)\dot{X}_h = M_{ei}(\Psi) \quad (18)$$

The over-all behavior of rotor blades in forward flight can be understood from the analysis of a two-degree-of-freedom system, where

$$X_1 = X_0 e^{\omega t} \quad (19)$$

and

$$Y_1 = Y_0 e^{\omega t} = \eta X_0 e^{\omega t} \quad (20)$$

Substituting Eqs. (19) and (20) into Eqs. (17) and (18) one can obtain the coupling ratio

$$\eta = -\frac{R_{11}(\Psi) + \omega S_{11}(\Psi)}{\omega^2 \alpha_{T1} + [\beta_{T1} + p_{11}(\Psi)]\omega + \gamma_{T1} + q_{11}(\Psi)} \quad (21)$$

and the polynomial

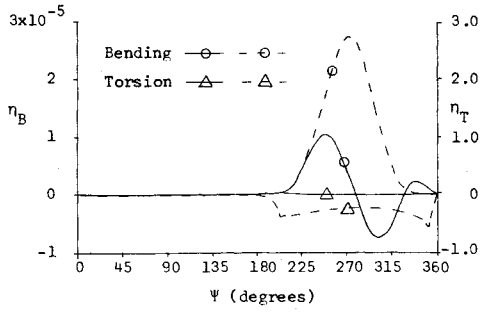

Fig. 11 Variation of coupling ratios for the torsional and bending modes with blade azimuth positions ($\kappa = 0.5$, $x_\theta = 0.0$, $\mu = 0.22$).

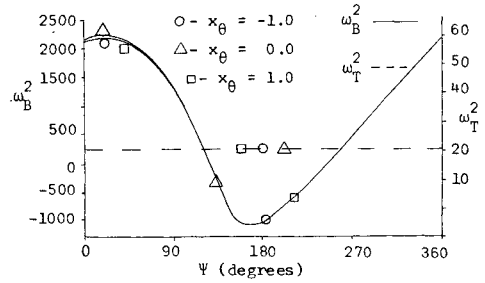

Fig. 12 Variation of natural bending and torsional frequencies with blade azimuth positions for various eccentricities between elastic and mass axes ($\kappa = 0.5$, $\mu = 0.22$).

$$\{\omega^2\alpha_{B1} + [\beta_{B1} + P_{11}(\Psi)]\omega + \gamma_{B1} + Q_{11}(\Psi)\}\{\omega^2\alpha_{T1} + [\beta_{T1} + p_{11}(\Psi)]\omega + \gamma_{T1} + q_{11}(\Psi)\} = m_{11}(\Psi)[R_{11}(\Psi) + \omega S_{11}(\Psi)] \quad (22)$$

Equation (22) is a 4th order polynomial, which can be solved to obtain the corresponding lowest frequencies of the coupled equations of motion. From Eq. (21) the degree of coupling can be calculated. Each one of the coefficients of Eqs. (21) and (22) has to be considered in order to understand the obtained results. According to the azimuth position of the blade, the coefficients in Eqs. (21) and (22) exhibit different characteristics. For a value of $\kappa = 0.5$ the coupled damping and stiffness terms (R_{11} and S_{11}) vanish in the forward flow region as shown in Fig. 8 and 9, and Eqs. (15) and (16) become uncoupled, as can be seen from Eq. (20). When the blade enters the reverse flow region, the magnitudes of the coupled terms (R_{ij} and S_{11}) vanish in the forward flow region as shown in Figs. 8 be analyzed from the complete solution of Eq. (20). It is also expected that in the reverse flow region the coupled frequencies will depend on the degree of coupling. As can be seen from Figs. 7 and 8, for the reverse flow region, the torsional frequency, ωT, depends on the negative aerodynamic stiffness and vanishing aerodynamic damping. If the coupling between bending and torsional modes is significant, the magnitudes of the torsional oscillations would be considerable for the coupled mode corresponding to the lowest bending frequency. The presence of torsional oscillations coupled with bending oscillations is indicated from the results of the harmonic analysis and from experimental measurements of pitching and plunging motion of rotor blades.[3]

Analysis of a Sample Blade in Forward Flight

The theoretical investigation of coupled torsional and bending vibrations of helicopter rotor blades was carried out for a sample blade (CH-34). A numerical solution was obtained from Eqs. (19) and (20) for varying blade properties and several flight conditions.[4,5] Figure 11 illustrates the coupling between torsional and bending vibrations of a rotor blade in forward flight for zero eccentricity between elastic and aerodynamic axes. For the operational speed of a CH-34 blade ($\mu = 0.22$), aerodynamic damping and natural bending frequency show a periodic variation with changing azimuth position, which can be explained from the variation of bending stiffness and damping coefficients in Figs. 4 and 5.[1] Torsional damping also varies periodically with changing azimuth positions. However, the constant torsional structural stiffness is the governing parameter in determining torsional frequency. The coupling ratio between the torsional and bending modes (η) exists in the reverse flow region and reaches a maximum value at the 270° position.

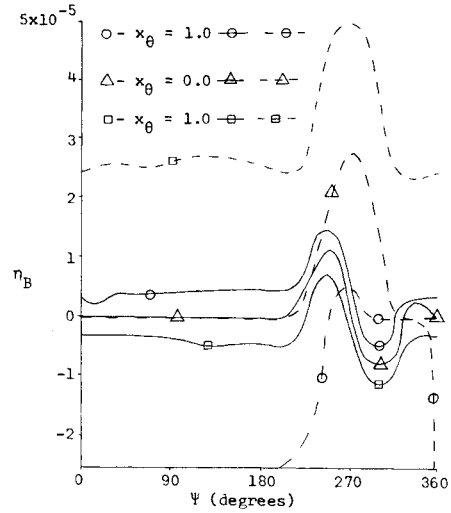

Fig. 13 Variation of coupling ratios for the bending mode with blade azimuth positions for various eccentricities between elastic and mass axes ($\kappa = 0.5$, $\mu = 0.22$).

The torsional sensitivity of rotor blades can be analyzed starting from the ideal uncoupled case. An important term to be included in a sensitivity analysis is the effect of the eccentricity between elastic and mass axes. The effect of structural coupling on blade sensitivity has been discussed above. The analysis can be repeated by adding the aerodynamic loading of the blade. As shown in Figs. 12 and 13, the bending and torsional frequencies, in this case, are not very sensitive to structural eccentricity. Such behavior can be attributed to the relative magnitudes of structural and aerodynamic coefficients. The variation of coupling ratio with eccentricities indicates its importance. The coupling in the bending mode is increased by a constant amount for all positions of the blade for an eccentricity of $x_\theta = -1$. However, for $x_\theta = 1$, it exists mostly in the forward flow region. The coupling ratio and the frequencies for the torsional modes were also increased with additional eccentricities. The second parameter to be considered in the torsional sensitivity analysis of rotor blades is the position of the aerodynamic axis with respect to the elastic center. For actual flight conditions, the exact position of an aerodynamic center would be a time-dependent parameter. A sensitivity analysis can be used as a guide, where the effects of changes in the aerodynamic and elastic axes can be analyzed both qualitatively and quantitatively. The above results were obtained for the ideal case, where the distance between the elastic and aerodynamic centers was one half chord width for both reverse and forward flow ($\kappa = 0.5$). The assumption that the rotor blade oscillates around the one-quarter chord width was used. In this case, the relative positions of the aerodynamic and elastic axes are moved in a symmetrical fashion by changing the values of κ to 0.4 and

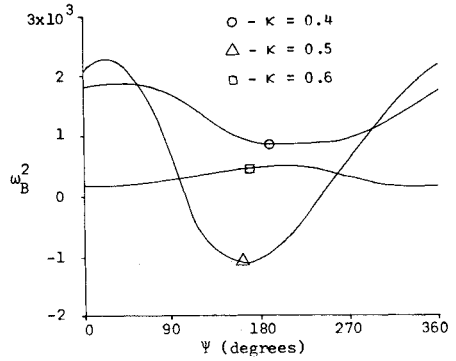

Fig. 14 Variation of natural bending frequency with blade azimuth positions for various eccentricities between elastic and aerodynamic axes ($x_\theta = 0.0$, $\mu = 0.22$).

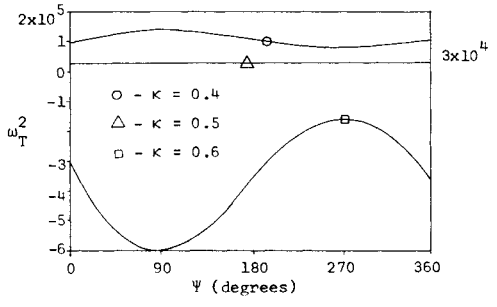

Fig. 15 Variation of natural torsional frequency with blade azimuth positions for various eccentricities between elastic and aerodynamic axes ($x_\theta = 0.0$, $\mu = 0.22$).

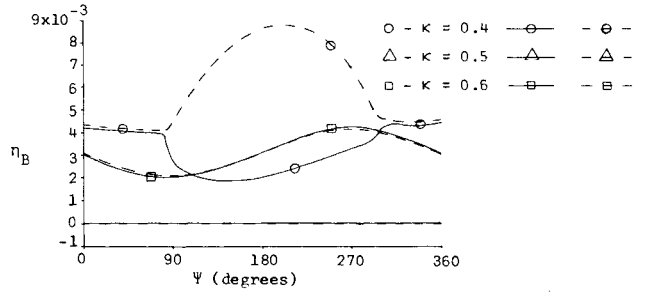

Fig. 16 Variation of coupling ratios for the bending mode with blade azimuth positions for various eccentricities between elastic and aerodynamic axes ($x_\theta = 0.0$, $\mu = 0.22$).

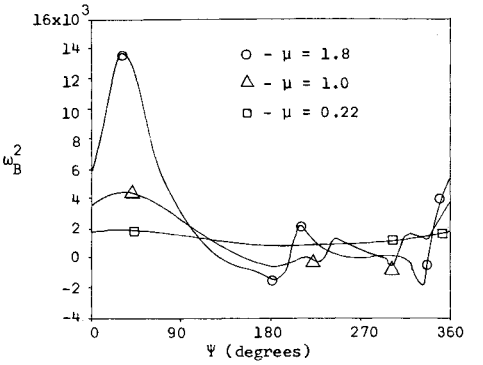

Fig. 17 Variation of natural bending frequency with blade azimuth positions for various tip-speed ratios ($\kappa = 0.4$, $x_\theta = 0.0$).

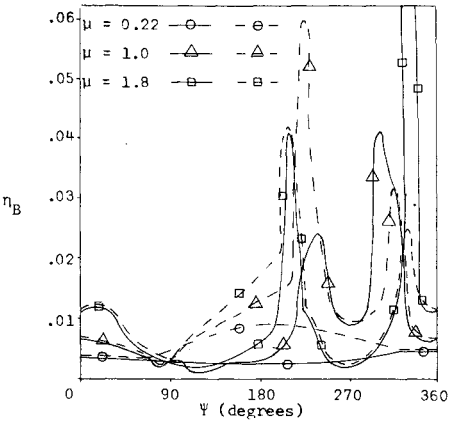

Fig. 18 Variation of coupling ratios for the bending mode with blade azimuth positions for various tip-speed ratios ($\kappa = 0.4$, $x_\theta = 0.0$).

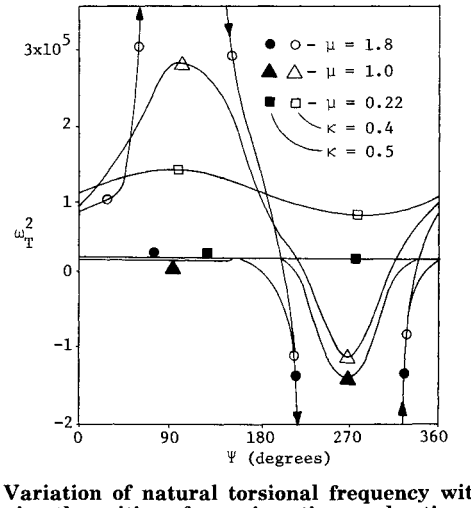

Fig. 19 Variation of natural torsional frequency with blade azimuth positions for various tip-speed ratios.

0.6, respectively. The aerodynamic pitching moments were redefined for varying positions of elastic and aerodynamic axes. The results are illustrated in Figs. 14–16.

For $\kappa = 0.6$ the bending frequencies of the rotor blade are reduced considerably for the entire rotor disk. For $\kappa = 0.4$ the frequencies have a much more consistent variation for different azimuth positions and demonstrate a stable behavior for azimuth position $90° < \Psi < 270°$ as compared to the case of $\kappa = 0.5$. Such behavior is due to the increase in stiffness obtained from the coupling with the torsional mode. The coupling ratio η, on the other hand, has been increased considerably compared to the uncoupled case. For the $\kappa = 0.4$ case, the coupling ratio is increased in the above region ($90° < \Psi < 270°$) and demonstrates an underdamped behavior. The variation of torsional frequencies with coupling between mass and elastic axes is also important. While the torsional frequencies are increased for $\kappa = 0.4$, the torsional mode becomes unstable for $\kappa = 0.6$. Such results indicate also that the blade vibrations will become unstable in a mainly torsional mode, when the aerodynamic center moves in front of the elastic center. The variation of coupling in the torsional mode indicates also a stable behavior of torsional vibrations which are overdamped for $\kappa = 0.4$.

The above results describe the sensitivity of vibration characteristics of the CH-34 blade at operating speeds ($\mu = 0.22$). Another important condition to be considered in

determining the torsional sensitivity of blades is the flight condition. The torsional and bending vibration characteristics were investigated for different flight conditions and different positions of aerodynamic and elastic axes. Figures 17 and 18 show the changes in frequencies and coupling for the bending vibrations of the blade. As the tip-speed ratio increases, the bending frequencies show a greater variation with changing azimuth positions. These results can be interpreted again from the behavior of bending stiffness terms shown in Fig. 4 for $\kappa = 0.5$. An instability region exists for the bending vibrations when $90° < \Psi < 180°$.[1] The bending frequencies remain low in the reverse flow region. The instability observed from the variation of coupling ratio for $180° < \Psi < 270°$ is due to the low torsional frequencies in this region. For $\kappa = 0.4$ the effect of the tip-speed ratios is considerably smaller, as a result of the aerodynamic coupling terms in bending and torsion. In the reverse flow region the bending frequencies change very rapidly at high tip-speed ratios as compared to the gradual change shown in the case of $\mu = 0.22$.

Variations of torsional vibration characteristics of rotor blades for different forward flight conditions are illustrated in Fig. 19. In the reverse flow region, the torsional frequencies are affected considerably. The negative torsional stiffness indicated in Fig. 7 causes an instability in the reverse flow region. The coupling ratio for the torsional mode shows an underdamped behavior and varies little with increasing tip-speed ratios. Torsional frequencies are also found to be sensitive to tip-speed ratios for $\kappa = 0.4$. Although the coupling has improved the torsional behavior compared to the uncoupled case ($\kappa = 0.5$), the torsional vibrations may still become unstable with increasing tip-speed ratios. The coupling ratio for this case indicates an underdamped behavior for high tip-speed ratios. For $\kappa = 0.6$, torsional vibrations are found to be unstable. As the tip-speed ratios increase, the torsional frequencies decrease proportionally. The coupling ratio for this case indicates an underdamped behavior and changes its sign in the forward and reverse flow regions.

Finally, a combination of eccentricities between elastic, mass, and aerodynamic centers was considered.[1] In this case, for $\kappa = 0.4$ and $\mu = 0.22$, the eccentricity x_θ was varied for $x_\theta = -1, 0, 1$. The bending and torsional frequencies were affected only slightly with this variation. This behavior is in accordance with the discussion of the relative magnitudes of structural and aerodynamic terms and their variation in defining vibration characteristics.

References

[1]Bratanow, T. and Ecer, A., "Sensitivity of Rotor Blade Vibration Characteristics to Torsional Oscillations," AIAA Paper 73-404, Williamsburg Va., 1973.

[2]Houbolt, J. C. and Brooks, G. W., "Differential Equations of Motion for Combined Flapwise Bending, Chordwise Bending, and Torsion of Twisted Non-Uniform Rotor Blades," TN 3095, 1957, NACA.

[3]Scheiman, J., "A Tabulation of Helicopter Rotor-Blade Differential Pressures, Stresses, and Motions as Measured in Flight," TM X-952, March 1964, NACA.

[4]Bratanow, T. and Ecer, A., "Sensitivity Analysis of Torsional Vibration Characteristics of Rotor Blades, Part I. Structural Analysis," CR 2379, March 1974, NASA.

[5]Bratanow, T. and Ecer, A., "Sensitivity Analysis of Torsional Vibration Characteristics of Rotor Blades, Part II. Aerodynamics and Sensitivity Analysis," CR 2380, March 1974, NASA.